Article

Journal of the Brazilian Chemical Society

https://dx.doi.org/10.21577/0103-5053.20240037

J. Braz. Chem. Soc. **2024**, *35*, 8, e-20240037, 1-17

Chemical Characterization and Evaluation of the Antitumoral Activity of *Annona tomentosa* R.E.Fr. on Breast (MCF-7) Three-Dimensional (3D) Tumor Spheroids

Aglaete A. Pinheiro,[a] Celina Y.-A. L. Lee,[b] Anna Gabriele P. dos Santos,[b] Érica R. Pereira,[b] Marcelino S. do Rosário,[c] Diego Luis Ribeiro,[d] Juliana Mara Serpeloni[b] and Cláudia Q. da Rocha *,[a]

[a]*Departamento de Química, Centro de Ciências Exatas e Tecnologia, Universidade Federal do Maranhão, 65080-805 São Luís-MA, Brazil*

[b]*Departamento de Biologia Geral, Centro de Ciências Biológicas, Universidade Estadual de Londrina (UEL), 86057-970 Londrina-PR, Brazil*

[c]*Departamento de Bioquímica e Química Orgânica, NuBBE, Instituto de Química, Universidade Estadual Paulista (UNESP), 14800-900 Araraquara-SP, Brazil*

[d]*Departamento de Microbiologia, Instituto de Ciências Biomédicas, Universidade de São Paulo (ICB/USP), 05508-000 São Paulo-SP, Brazil*

Annona tomentosa, popularly known as "*araticum marolo*", is an Annonaceae with little scientific evidence regarding its phytochemistry and biological activities. Based on this, the present study carried out the chemical characterization of the methanolic extract and fractions of ethyl acetate and alkaloid of the stem bark of *A. tomentosa*, in addition to evaluating their influence on the viability, proliferation and migration of breast (MCF-7) cells in a three-dimensional (3D) model. The samples were analyzed by liquid chromatography-tandem mass spectrometry (LC-MS/MS), and the Global Natural Products Social Networking (GNPS) platform was used to construct a molecular network. 21 compounds were identified, of which 16 belong to the alkaloid class. Multicellular spheroids (MCTS) growth was reduced after 216 h of treatment, as well as their viability (ca. 50% for the extract and ca. 25% for the alkaloid fraction). The extract and the alkaloid fraction showed greater antiproliferative (at a concentration of 100 μg mL^{-1} after 216 h, ca. 48% for the extract and ca. 20% for the fraction) and antimigratory (at concentrations 50-500 μg mL^{-1} for the extract and 100-250 μg mL^{-1} for the fraction) effects. This study is pioneering in demonstrating the antitumor effects in a 3D culture model, also revealing its potential for the isolation of alkaloids.

Keywords: Annonaceae, phytochemistry, GNPS, alkaloid, anticancer

Introduction

Plants are the basis of traditional medicine worldwide due to the production of bioactive substances. One of the most investigated genera is the *Annona* due to its biological potential. Its species are reported for anticancer, anti-inflammatory, antioxidant, and antimicrobial activities. Among some types of molecules attributed to the pharmacological potential of the genus are terpenoids, flavonoids, acetogenins, alkaloids, tannins, and phenols, isolated mainly from leaves, bark, stems, and fruits. Research points out that annonaceous acetogenins and alkaloids are bioactive and are most effective against tumor cell lines, such as breast cancer, which is one of the main public health problems.[1-3]

According to the Global Cancer Observatory (GCO),[4] the estimated number of new cases in 2020 was 2,261,419 globally, compared to both sexes and at all ages, surpassing the number of lung cancer cases. Of these cases, 684,996 resulted in death, corresponding to the most frequent cause of death from cancer in women.[4] According to Merino Bonilla *et al.*[5] and Kashyap *et al.*,[6] this increase in incidence, when compared to the previous centuries, may be related to the rise in the exposure of the population to risk factors, such as lifestyle, alcoholism, obesity, prolonged exposure to non-estrogenic and estrogenic mutagenic agents, and especially the aging.

*e-mail: rocha.claudia@ufma.br
Editor handled this article: Hector Henrique F. Koolen (Associate)

To treat the disease and prevent the formation of metastases, surgeries are generally performed to remove the tumor mass and axillary lymph nodes, with or without adjuvant and neoadjuvant treatments, such as chemotherapy and radiotherapy.[7,8] However, the difficulty of treatment in more advanced stages and the side effects in the short and long term,[9-11] indicate the need to search for new compounds that help both in chemoprevention and in the treatment.

Studies[12-16] carried out with *Annona* species have demonstrated cytotoxic and antiproliferative potential in different cancer cell lines. *Annona squamosa* leaf extracts showed *in vitro* and *in vivo* antiproliferative and cytotoxic effects against two breast cancer cell lines: MCF-7 and MDA-MB-231.[12] In MCF-7 cells, *Annona squamosa* induced apoptosis, generation of reactive oxygen species (ROS), and intracellular glutathione decrease.[13,14] The extracts and fractions from the *Annona muricata* plant demonstrated cytotoxic effects in MCF-7 cells mediated by the downregulation of anti-apoptotic proteins (for example, BCL-2) and by the upregulation of pro-apoptotic enzymes (i.e., caspases).[15] Similarly, *in vitro* studies with *Annona cherimola* in MDA-MB-231 cells highlighted its antiproliferative and pro-apoptotic effects through activation of the apoptosis intrinsic pathway through the release of cytochrome c and the increase in pro-apoptotic and p21 proteins.[16]

Annona tomentosa R. E. Fr., popularly known as "*araticum marolo*",[17] is an Annonaceae native and not endemic in Brazil. The literature reports the antinociceptive and anti-inflammatory activity of the leaf extract,[18] as well as some phytoconstituents also from the leaf extract: kaempferol-3-*O*-rhamnosylglucoside, quercetin-3-*O*-glucoside, quercetin-3-*O*-rhamnosylglucoside and luteolin-7-*O*-glucoside.[19]

Thus, considering the biological potential of the *Annona* species mainly against breast cancer cells, the aim of this work was to evaluate the chemical composition of the methanolic extract, ethyl acetate and alkaloid fractions of the stem bark of *A. tomentosa* by liquid chromatography-tandem mass spectrometry (LC-MS/MS) and build molecular networking through the Global Natural Products Social Networking (GNPS) platform, in addition to investigating the cytotoxic activity of the samples in MCF-7 cells cultured in three-dimensional (3D) spheroids models.

Experimental

Collection of plant material

Annona tomentosa stem bark was collected on September 26, 2020, in the village of Morro Grande, located in the municipality of Vargem Grande, Maranhão, Brazil, under the coordinates 03°32'06.0"S and 43°56'48.7" W. The plant was identified in the Rosa Mochel Herbarium at the State University of Maranhão by Prof Ana Maria Maciel Leite. The specimen was deposited under No. 3773. Access to the National System for the Management of Genetic Heritage and Associated Traditional Knowledge (SisGen) was registered under code No. A039D1F.

Obtaining the methanolic extract of *Annona tomentosa* R.E.Fr.

The plant material was dried in an oven (Hexasystems, SSDic, São Paulo, Brazil) at 40 °C for 72 h and ground in a knife mill using a 1.0 mm mesh. The powder obtained (1350.0 g) was subjected to an extraction process with methanol (Êxodo Científica, Campinas, Brazil) (3800.0 mL) by the maceration method. Initially, sample extraction was maintained for one week. Subsequently, the solvent renewal was performed twice more, every 72 h. The solvent was evaporated from the extract using reduced pressure and controlled temperature (40-50 ºC) and reused at each maceration stage. At the end of the process, the plant extraction residue was discarded. The sample obtained was lyophilized (Liotop freeze dryer, K105, São Carlos, Brazil) to remove the solvent. The methanolic extract then presented a mass equal to 273.36 g. The yield was 20.25%.

Liquid-liquid partition of the extract

Ethyl acetate fraction

The ethyl acetate fraction was obtained from the dissolution of 20.0 g of methanolic extract in water/methanol (7:3) (200.0 mL) and partition with ethyl acetate (Êxodo Científica, Campinas, Brazil) (100.0 mL), after five extractions, with an interval of 24 h each. Then, the acetate fraction was lyophilized (Liotop freeze dryer, K105, São Carlos, Brazil) to remove the solvent. After complete drying, the fraction had a mass equal to 4.0 g. The yield was 20.0%.

Acid-base extraction (alkaloid fraction)

The methanolic extract (20.0 g) was dissolved in water/methanol (7:3) (100.0 mL) and acidified with 37% HCl solution (3 mL) (Êxodo Científica, Campinas, Brazil) until pH 2.0. The obtained solution was partitioned with ether (100.0 mL). The remaining aqueous phase containing the bulk extract was basified to pH 11 with NH_4OH solution (20 mL) (Êxodo Científica, Campinas, Brazil) and partitioned with $CHCl_3$ (100 mL) (Synth, Campinas, Brazil). The chloroform (alkaloidal phase) was concentrated on a rotary evaporator (Quimis, Diadema,

Brazil) and lyophilized (Liotop freeze dryer, K105, São Carlos, Brazil) to remove solvents. The fraction had a mass of 0.860 g. The yield was 4.3%. To confirm the presence of alkaloids, thin-layer chromatography (TLC) was performed with a dichloromethane/methanol (DCM/MeOH) (Êxodo Científica, FURLAB, Campinas, Brazil) (9:1) elution system, using Dragendorff's reagent and UV light (Sppencer®, Hipperquímica, Iperó, Brazil) (254 nm).[20]

For use in cell culture, the treatments were diluted 200 times, obtaining concentrations between 10 and 500 μg mL^{-1} in culture for the methanolic extract and concentrations between 10 and 250 μg mL^{-1} in culture for the alkaloidal and acetate fractions. The concentrations used in this study were based on the solubility of the extract and its fractions in dimethyl sulfoxide (Synth, FURLAB, Campinas, Brazil) (0.25% DMSO).

HPLC-UV-Vis analysis

The crude extract and the ethyl acetate and alkaloid fractions of *Annona tomentosa* were analyzed by high-performance liquid chromatography with ultraviolet-visible (HPLC-UV-Vis) detection. A cleaning step was performed to remove any contaminants. The sample solutions (10 mg mL^{-1}, 1 mL) underwent solid phase extraction (SPE) using Phenomenex Strata C18 cartridges (500.0 mg of stationary phase) previously activated with 5.0 mL of MeOH and then equilibrated with 5.0 mL of MeOH:H_2O (1:1, v v^{-1}). Samples were filtered through a 0.22 μm polytetrafluoroethylene (PTFE) filter and dried. The dried samples were dissolved at a concentration of 10.0 mg mL^{-1} in HPLC grade methanol solvent. Aliquots of 20.0 μL were injected directly into the HPLC-UV-Vis with detection at 277 nm.

A Shimadzu model HPLC system (Shimadzu Corp., Kyoto, Japan) was used, consisting of a solvent injection module with a binary pump, and UV-Vis detector (SPA-10A). The column used was Luna 5.0 μm C18 100 A (150.0 μm × 4.6 μm). The elution solvents were A (2% acetic acid in water) and B (methanol). The extract was eluted with the following gradient: 2 to 100% B in 35 min, and the fractions in the gradient: 5 to 100% B in 70 min. The flow was 1 mL min^{-1}, the column temperature was 20 ºC. The injection volume of the samples was 20.0 μL. Data were processed using LC Solution 2.3 software (Shimadzu).[21]

Liquid chromatography-mass spectrometry (LC-MS) analysis

Chemical characterization was performed by liquid chromatography-electrospray ionization ion trap mass spectrometry (LC-ESI-IT-MS) with a spectrometer (amaZon SL Bruker Daltonics®, Massachusetts, USA). The chromatographic analysis was performed on a Luna 5 μm C18 100 Å column (250 × 4.6 mm, Phenomenex, Torrance, USA), with HPLC Prominence Shimadzu®. The binary gradient mobile phase consisted of 0.1% formic acid (Sigma-Aldrich, St. Louis, LO, USA) in water (solvent A) and 0.1% formic acid in methanol (Sigma-Aldrich, St. Louis, LO, USA) (solvent B). Samples (1 mg mL^{-1}) were eluted from the analytical column with a 40 min gradient ranging from 5 to 100% solvent B at a constant 1 mL min^{-1} flow rate. The injection volume was 2 μL. Column compartment temperature set to 40 °C.

Data acquisition was performed in positive ionization mode, with fragmentation in multiple stages (MS^2 and MS^3), according to the following parameters: nebulization gas pressure, 50.0 psi; capillary temperature, 300 °C; transfer capillary input voltage, 4500 V; desolvation gas, nitrogen (N_2), flow 10 L min^{-1}; collision gas, helium (He); range acquisition, *m/z* 50-1200. Raw data were analyzed using Data Analysis 4.3 software (Bruker, Massachusetts, USA).[22]

MS/MS data processing and molecular networking

The raw data acquired in ".d" in the positive mode were converted to ".mzML" using DataAnalysis (Bruker). These files were uploaded to the GNPS platform to generate molecular networking.

Molecular networks were created using the GNPS platform.[23] The data were filtered by removing all MS/MS fragment ions within 17 Daltons (Da) of the precursor *m/z*. The MS/MS spectra were window filtered by choosing only the top 6 fragment ions in the 50 Da window across the spectrum. The precursor ion and MS/MS fragment ion mass tolerances were adjusted to 0.5 Da. A network was created where edges were filtered to have a cosine value above 0.7 and more than four matching peaks. The maximum size of a molecular family was defined as 100. The spectra were then searched against the GNPS spectral libraries. All matches maintained between network and library spectra needed a score above 0.7 and at least four matching peaks.[24] The network visualization was performed using the Cytoscape 3.9.1 software.[25]

Cell culture and treatments

The experimental model was the breast tumor cell line MCF-7 (ATCC® HTB-22™), derived from metastatic breast adenocarcinoma isolated from the mammary gland. The cells were cultivated in complete Dulbecco's Modified

Eagle Medium (DMEM) medium supplemented with 10% fetal bovine serum (FBS) and with 1% antibiotics penicillin (0.06 g L^{-1}, CAS: 69-57-8) and streptomycin (0.10 g L^{-1}, CAS: 3810-74-0), all reagents obtained from Gibco (Grand Island, New York, USA). The cells were grown in 25 cm^2 cell culture bottles at 37 ºC in an atmosphere containing 5% CO_2 and 95% relative humidity. After reaching 80-90% confluence, the cells were sub-cultured. All experiments were performed with aliquots between the 3rd and 8th cell passages.

The cells were treated with different concentrations of the methanolic extract (10, 50, 100, 200, 300, 400, and 500 µg mL^{-1}), ethyl acetate fraction (10, 50, 100, 150, 200, and 250 µg mL^{-1}), and alkaloid fraction (10, 50, 100, 150, 200, and 250 µg mL^{-1}) concentrations. The extract and fractions were solubilized in dimethyl sulfoxide (DMSO 0.25%, final concentration in culture).

Formation of 3D tumor multicellular spheroids (MCTS)

MCTS were generated by seeding 5000 cells *per* well in 200 µL of complete DMEM medium in the ultra-low attachment (ULA) 96-well round-bottomed plates (Greiner bio-one, Cat. No. 655 180; Frickenhausen, Germany) and cultured for 2 days at standard culture conditions as previously standardized.[26] After that, MCTS photomicrographs were obtained using the Olympus CKX41 inverted microscope image capture system with a 4× objective, using the Qimaging Pro 7.1 software (Teledyne, Canada),[27] and then analyzed using the Zen 2.3 software (Zeiss, Germany) with the "measure" tool.[28] After capturing the images, the MCTS were treated with solvent control (DMSO 0.25%), methanolic extract (10, 50, 100, 200, 300, 400, and 500 µg mL^{-1}), or alkaloidal and ethyl acetate fractions (10, 50, 100, 150, 200, and 250 µg mL^{-1}) and positive control docetaxel (DTX 100 µM). All treatments were performed by replacing 50% of the culture supernatant with a 2× drug-supplemented culture medium.

Cell viability (resazurin)

Evaluation of cell viability through the resazurin reduction assay (Sigma-Aldrich, St. Louis, USA) was performed according to the protocol described by Walzl *et al.*,[29] after 72 and 216 h of treatments. After treatments, a resazurin working solution (0.015 mg mL^{-1} diluted in phosphate-buffered saline (PBS) solution) was added at 20% of the final volume (40 µL) to each well containing the 3D tumor spheroids. The plates were incubated for 24 h at 37 ºC, and absorbances were measured in a microplate reader (Biotek Elx800) at λ = 570 nm for resofurin and λ = 600 nm for resazurin. The absorbances obtained were multiplied by the oxidation factor at each wavelength (117216 for wavelength 570 nm and 80586 for wavelength 600 nm) and subtracted from converted resofurin, and the percentage cell viability was calculated by normalizing the absorbance of each treatment with the solvent control (SV) considered 100%.

Cell death (necrosis)

Necrotic cells were analyzed using propidium iodide (PI) (Thermo Fischer Scientific, Waltham, USA) dye, following the instructions of the manufacturer. After the resazurin assay (96 h), the spheroids were labeled with the PI (40 µg mL^{-1} in PBS) and Hoechst 33342 (30 µg mL^{-1} in PBS) for 1 h and 30 min, and the samples were analyzed. All images of MCF-7 were performed 96 h after treatments by fluorescence microscopy using the EVOS XL Core Imaging System image capture system in the RFP channel (channel 2 red/PI; channel 3 DAPI (4'-6-diamidino-2-phenylindole, dihydrochloride)/ Hoechst 33342), and the plates scanned using the "one field of view *per* well" acquisition mode with the 10× objective. The acquired images were analyzed using Fiji v.3.1 using the "Color Automatic Histogram counting" macro after background adjustment by the "image threshold".[30] Necrotic cells were quantified using the "average fluorescence intensity" recorded on the red channel. Representative images from MCF-7 spheroids were acquired with Hoechst (blue) and PI (red) merged.

Volume, morphology, and integrity analysis of MCF-7 3D tumor spheroids

The structure, growth kinetics, integrity, and area of each MCF-7 spheroid have been analyzed according to Friedrich *et al.*[31] and Vinci *et al.*[32] The treatments were performed, and the photomicrographs were obtained at 0 (day 3 after initiation), 72, 144, and 216 h after treatments using an Olympus CKX41 inverted microscope with a 4× objective, with the aid of the Qimaging Pro 7.1 software (Teledyne, Canada).[27] After capturing the images, 100 µL of the contents of all wells were removed, and then 100 µL of 2× treatments diluted in DMEM medium were added to replace nutrients and treatments. In the integrity/morphology assessment, each image obtained was evaluated for detecting irregular spheroids (without a circular shape), with cellular disaggregation or irregular cell agglomeration to analyze the integrity and morphology of the 3D spheroids. For volume and growth analysis, the circumference of the spheroid was measured using the

Zen 2.3 software (Zeiss, Germany) with the "measure" tool.[28] The area comprised by the spheroid was presented in μm^3. At the end of the integrity test, the resazurin solution was added for viability analysis after 216 h of treatment, as described in "Resazurin" sub-section.

3D clonogenicity assay

The clonogenic assay was performed following the protocol by Mikhail *et al.*,[33] and standardized by Ribeiro *et al.*[34] After 72 h of treatments, the MCF-7 spheroids and supernatants were transferred to a 2.0 mL microtube and centrifuged at 2500 rpm for 5 min. Then, the supernatant was discarded and trypsinized, and 300 viable cells were seeded in 6-well plates (Greiner bio-one, Cat. No. 657 160; Frickenhausen, Germany) with 5 mL of complete culture medium in each well. The plates remained in an incubator for 10 days until the colonies were fixed for 30 min in methanol:acetic acid:distilled water (1:1:8 mL; v/v/v; Sigma-Aldrich, St. Louis, USA) and stained for 5 min with 5% Giemsa diluted in phosphate buffer (1:20 mL; v/v).[35] The colonies were counted, according to the protocol by Franken *et al.*,[36] with the aid of a binocular stereomicroscope, and the results were normalized in relation to the SV, considered with a surviving fraction (SF) = 100%.

3D cell migration in extracellular matrix

The cell migration from the MCF-7 spheroids to the extracellular matrix (ECM) was evaluated in gelatin from bovine skin (CAS: 9000-70-8, Sigma-Aldrich, St. Louis, USA) as described by Vinci *et al.*[37] Initially, 50 µL of 0.02% gelatin solution was pipetted *per* well into 96-well plates, which remained at room temperature for 3 h to fix the extracellular matrices at the bottom of the well. Then, the remaining non-adherent volume was carefully removed, the wells were washed twice with PBS, and 100 µL of bovine serum albumin blocking solution (BSA) at 1% (m/v) diluted in PBS was added. The plates were kept at rest for 1 h until the MCF-7 spheroids were transferred and treatments added. The photomicrographs of the 3D spheroids were performed at 0, 24, 48, 72, and 96 h in an inverted microscope Olympus CKX41 with a 4× objective, with the aid of the Qimaging Pro 7.1 software.[27] The 3D cell migration analysis was performed by measuring the area occupied by cells that migrated from the spheroid using the AxioVision 3.1 software (Zeiss, Germany) with the "measure" tool,[38] and the areas were presented in μm^2. For confirmation of cell death in cell migration experiments, after 72 h of treatment, the dyes Hoestch and PI (30 µg mL^{-1} Ho and 40 µg mL^{-1} PI) were added and then incubated for 1 h and 30 min in a dark environment. Finally, the MCF-7 spheroids and cell migration areas were photographed and analyzed by the EVOS® FL fluorescence microscope (Thermo Fischer Scientific, Waltham, USA) in a 10× objective for representative images.

Statistical analysis

All the experiments described were performed in three biological replicates (n = 3). The results of the biological assays obtained after treatments with the methanolic extract, its fractions, and its respective controls (solvent and positive) were initially submitted to data distribution analysis (normality test) by the Shapiro-Wilk test. For tests in which the results demonstrate non-parametric distribution, the Kruskal-Wallis test followed by the Dunnet post hoc test was performed to analyze results, considering values $p \leq 0.05$ as significant. For samples with parametric distribution, data were analyzed using the analysis of variance (ANOVA) test followed by Dunnett's, considering $p \leq 0.05$ as significant. All statistical analyzes were performed using the GraphPad Prism 7.0 software (La Jolla, USA).[39]

Results and Discussion

To analyze the chromatographic profile of the main substances in the extract and ethyl acetate and alkaloid fractions of *A. tomentosa*, the chemical profile of the samples (extract and ethyl acetate and alkaloid fractions) was obtained by high-performance liquid chromatography (HPLC-UV-Vis) (Figure 1). Overlaid UV-Vis chromatograms at 277 nm are shown in Figure 2.

From the mass spectra of the samples obtained by LC-MS, it was possible to propose 21 compounds (Figure 3) for *A. tomentosa*. The data acquired from the compounds in negative and positive modes, such as retention time, fragmentation, and identification, are presented in Table 1.

Based on the results, the chemical profiles of the methanolic extract, acetate, and alkaloid fractions of *Annona tomentosa* showed the predominance of compounds from the alkaloid classes, concentrated primarily in the alkaloid fraction.

Alkaloids **3** and **4**, molecular ion *m/z* 316 $[M + 2H]^+$ (Figures S3 and S4, Supplementary Information (SI) section), were suggested as oblongine isomers. MS^2 spectra provided characteristic fragments at *m/z* 269 and 192, which may be associated with the loss of *N*-dimethylamine and the isoquinoline fragment, respectively. Furthermore, in the MS^3 spectra, it was possible to observe fragment ions

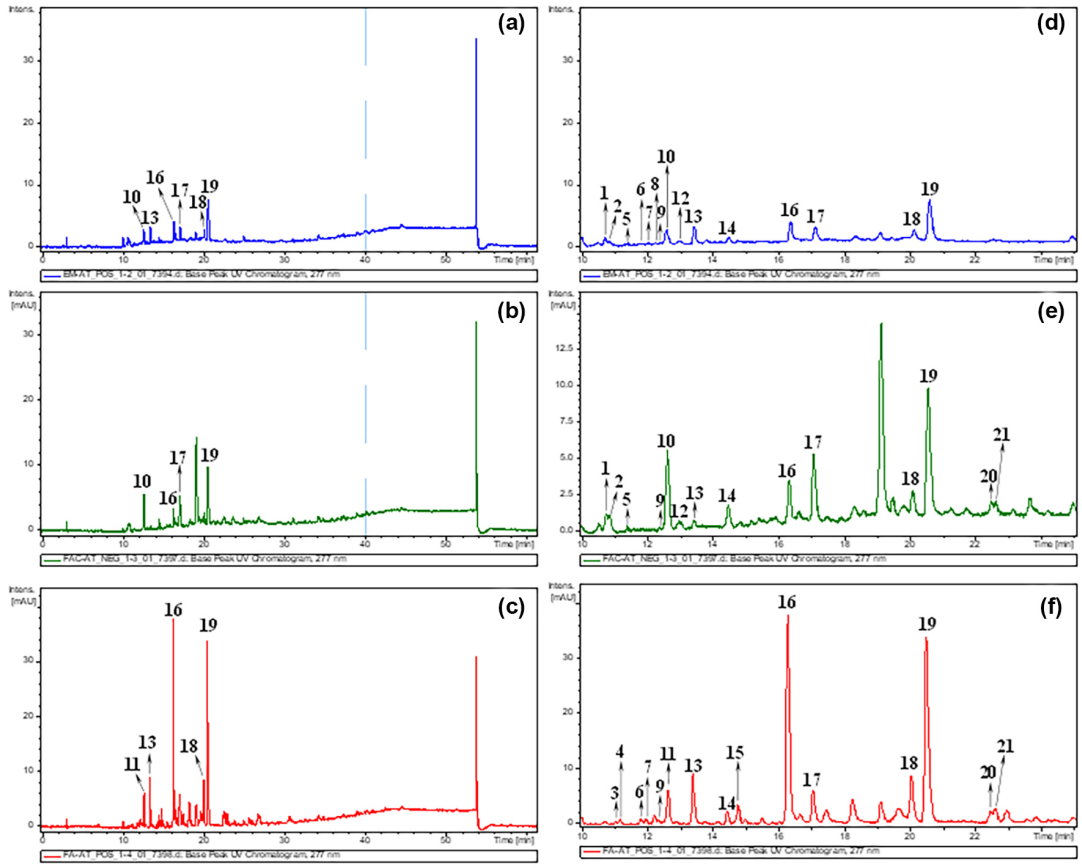

Figure 1. UV-Vis chromatograms at 277 nm of the extract and ethyl acetate and alkaloid fractions of *Annona tomentosa*. (a) Total chromatogram of the extract; (b) total chromatogram of the ethyl acetate fraction; (c) total chromatogram of the alkaloid fraction; (d) chromatogram of the expanded extract; (e) chromatogram of the expanded ethyl acetate fraction; (f) chromatogram of the expanded alkaloid fraction. The expansion of the chromatograms (d); (e) and (f) was carried out in the retention time range of 10 to 25 min.

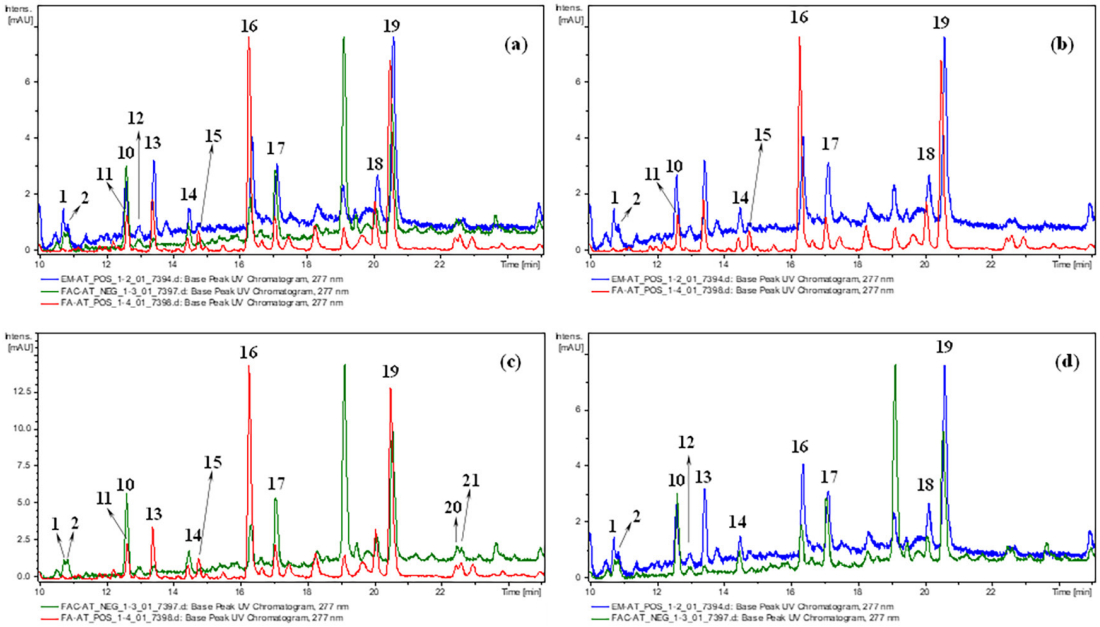

Figure 2. UV-Vis chromatograms at 277 nm, expanded in the time range of 10 to 25 min, superimposed of the extract and ethyl acetate and alkaloid fractions of *Annona tomentosa*. (a) Overlap between the chromatograms of the extract (in blue), with those of the ethyl acetate fraction (in green) and the alkaloid fraction (in red); (b) overlap between the chromatograms of the extract (in blue) with that of the alkaloid fraction (in red); (c) overlap between the chromatograms of the ethyl acetate fraction (in green) with that of the alkaloid fraction (in red); (d) overlap between the chromatograms of the extract (in blue) with that of the ethyl acetate fraction (in green).

Table 1. Compounds identified in the extract and in the ethyl acetate and alkaloid fractions of *Annona tomentosa*

Peak	Retention time / min	Compound	Mode		Fragment (*m/z*)	EM	FAC	FA	Reference
1	10.7	procyanidin dimer type B (isomer I)	–	MS^2	577 $[M - H]^-$; 559; 451; 425; 407; 289	×	×	–	40
				MS^3	577→425: 407				
			+	MS^2	579 $[M + H]^+$; 427; 409; 301; 291				
				MS^3	579→427: 409; 301; 275				
2	10.9	procyanidin dimer type B (isomer II)	–	MS^2	577 $[M - H]^-$; 559; 451; 425; 407; 289	×	×	–	40
				MS^3	577→425: 407				
			+	MS^2	579 $[M + H]^+$; 427; 409; 301; 291				
				MS^3	579→427: 409; 301; 275				
3	11.1	oblongine (isomer I)	+	MS^2	316 $[M + 2H]^+$; 269; 192	–	–	×	41
				MS^3	316→269: 237; 209; 175; 145; 137; 107				
4	11.2	oblongine (isomer II)	+	MS^2	316 $[M + 2H]^+$; 269; 192	–	–	×	41
				MS^3	316→269: 237; 209; 175; 145; 137; 107				
5	11.6	procyanidin trimer type B	–	MS^2	865 $[M - H]^-$; 847; 695; 577; 543; 425; 287	×	×	–	42
				MS^3	865→577: 559; 467; 451; 407; 331; 289; 243				
6	11.8	stepholidine	+	MS^2	328 $[M + H]^+$; 178	×	–	×	43
7	12.0	*N*-methylisococlaurine	+	MS^2	300 $[M + H]^+$; 269	×	–	×	44
				MS^3	300→269: 237; 209; 175; 145; 137; 107				
8	12.2	tembetarine	+	MS^2	344 $[M]^+$; 299 175	×	–	–	45
				MS^3	344→299: 267; 235; 175; 143; 137				
9	12.3	coclaurine	+	MS^2	286 $[M + H]^+$; 269	×	×	×	46
				MS^3	286→269: 237; 175; 145; 137; 107				
10	12.6	catechin[a]	–	MS^2	289 $[M - H]^-$; 245; 205; 179	×	×	–	47-49
				MS^3	289→245: 227; 203				
			+	MS^2	291 $[M + H]^+$; 273; 165; 139; 123				
11	12.7	benzylisoquinoline alkaloid (isomer I)[a]	+	MS^2	346 $[M + H]^+$; 299	–	–	×	50
				MS^3	346→299: 267; 235; 175; 143; 137				
12	13.0	procyanidin dimer type B (isomer III)	–	MS^2	577 $[M - H]^-$; 509; 451; 425; 407; 289	×	×	–	40
				MS^3	577→425: 407				
13	13.5	reticuline	+	MS^2	330 $[M + H]^+$; 192	×	×	×	51
				MS^3	330→192: 177				
14	14.5	cyclanoline	+	MS^2	342 $[M]^+$; 192	×	×	×	45
				MS^3	342→192: 190; 177				
15	14.8	benzylisoquinoline alkaloid (isomer II)	+	MS^2	346 $[M + H]^+$; 299	–	–	×	50
				MS^3	346→299: 267; 235; 175; 143; 137				
16	16.4	asimilobine	+	MS^2	268 $[M + H]^+$; 251; 219	×	×	×	43,51
				MS^3	268→251: 219				
17	17.2	tetrahydropamatine	+	MS^2	356 $[M]^+$; 192	×	×	×	45
				MS^3	356→192: 192; 177				
18	20.2	nornuciferine	+	MS^2	282 $[M + H]^+$; 265	×	×	×	43
				MS^3	282→265: 250; 234				
19	20.6	anonaine	+	MS^2	266 $[M + H]^+$; 249	×	×	×	43,52
				MS^3	266→249: 219; 191				
20	22.4	xylopine	+	MS^2	296 $[M + H]^+$; 279	–	×	×	51
				MS^3	296→279: 264; 249; 234; 221				
21	22.6	*O*-methylisopiline	+	MS^2	312 $[M + H]^+$; 295	–	×	×	43
				MS^3	312→295: 280; 264; 221				

[a]The peak at 12.6 min showed the same fragmentation in both positive and negative modes, of the samples referring to the extract and the ethyl acetate fraction, indicating that it was catechin, however, the peak at 12.7 min that appears in the fraction alkaloid, showed a similar mass spectrum to an unidentified benzoisoquinoline alkaloid. EM: extract; FAC: ethyl acetate fraction; FA: alkaloid fraction; ×: present in the sample; –: absent in the sample.

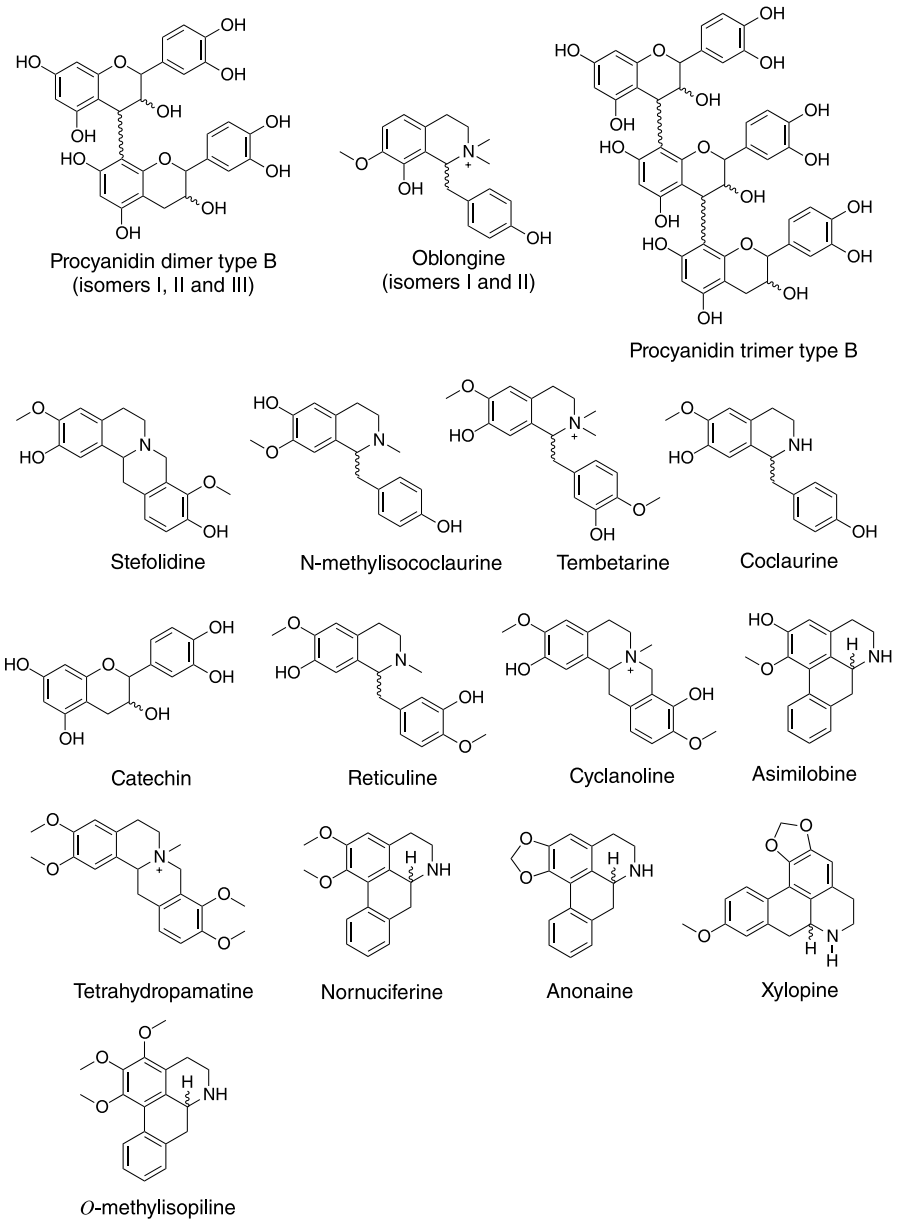

Figure 3. Compounds identified in the extract and the ethyl acetate and alkaloid fractions of *Annona tomentosa*.

at *m/z* 237, 175, and 107 related to the loss of the methanol portion, the benzene portion, and the benzylic cleavage fragment, respectively.[41] This compound has already been reported for other Annonaceae species.[46,53]

Compound **6**, molecular ion *m/z* 328 $[M + H]^+$ (Figure S6, SI section), was proposed as stepholidine, a tetrahydroprotoberberine alkaloid. According to de Lima *et al.*,[43] the fragment ion *m/z* 178 was possibly produced by RDA (Retro-Diels-Alder), representing the methoxyl and hydroxyl groups of ring A. The neutral loss of 150 Da may also be related to the presence of methoxyl and hydroxyl groups in the D ring.

The molecular ion *m/z* 300 $[M + H]^+$ (Figure S7, SI section) was exhibited by compound **7**. The compound was proposed as *N*-methylisococlaurine. Fragment ion at *m/z* 269 suggests the compound is an *N*-methyl tertiary amine due to loss of CH_3NH_2. This fragmentation pattern was also reported by Lin *et al.*[44]

Compound **8**, molecular ion *m/z* 344 $[M + H]^+$ (Figure S8, SI section), was proposed as tembetarine, a benzylisoquinoline alkaloid. Fragment ions at *m/z* 299 and 267 correspond to losses of $(CH_3)_2NH$ (–45 Da) and $(CH_3)_2NH - CH_3OH$ (–77 Da), respectively. Additional fragment ions at *m/z* 137 and 175 were observed. According to Jiao *et al.*,[45] the fragment ion at *m/z* 137 was generated from α cleavage at position 8.9 of the molecular ion, while *m/z* 175 was obtained through α-cleavage fragmentation from 9,10-position of *quasi*-molecular ions.

Similar to compound **8**, compounds **11** and **15**, *m/z* 346 $[M + H]^+$ (Figures S11 and S15, SI section), exhibited fragment ions at *m/z* 299, 267, 175 and 137. Therefore, they were proposed as benzylisoquinoline alkaloid isomers.[50]

Compound **9**, *m/z* 286 $[M + H]^+$ (Figure S9, SI section), was suggested as coclaurine, an intermediate in the biosynthesis of the benzylisoquinoline alkaloid.[54,55] Fragment ions at *m/z* 269 and 237 were observed to be associated with the respective losses of NH_3 and CH_3OH. Skeletal cleavage also produced intense fragment ions at *m/z* 175 and 107, as reported by Lima *et al*.[46]

The molecular ion *m/z* 330 $[M + H]^+$ (Figure S13, SI section) was exhibited by compound **13**. The compound was proposed as reticuline, a biosynthetic precursor of aporphine alkaloids. Fragment ion was observed at *m/z* 192 due to the isoquinoline portion of the tertiary amine disubstituted by methoxy and hydroxyl groups. Furthermore, fragment ion at *m/z* 177 was also observed. This fragmentation pattern was also reported by Macedo *et al*.[51]

Compound **14** generated the $[M + H]^+$ ion at *m/z* 342 (Figure S14, SI section). The ion at *m/z* 192 generated suggests the occurrence of a RDA cleavage. Fragment ions at *m/z* 190 $[M - 150 - 2H]^+$ and 177 $[M - 150 - CH_3]^+$ were also observed. According to a literature report,[45] this compound was inferred as cyclanoline, an *N*-methyltetrahydroprotoberberine-type alkaloid.

Molecular ions *m/z* 268 $[M+H]^+$ (Figure S16, SI section), *m/z* 282 $[M + H]^+$ (Figure S18, SI section), *m/z* 266 $[M + H]^+$ (Figure S19, SI section) and *m/z* 312 $[M + H]^+$ (Figure S21, SI section) were assigned to compounds **16**, **18**, **19** and **21** suggested as asimilobine, nornuciferine, anonaine and *O*-methylisopiline, respectively, common aporphine alkaloids in Annonaceae species.[56-58]

Fragment ions at *m/z* 251 and 249 were generated after the loss of NH_3 in compounds **16** and **19**, respectively, and subsequent losses of CH_3OH and CO. For compound **18**, fragment ions were observed at *m/z* 265, 250, and 234, attributed to losses of 17 Da (– NH_3), 15 Da (– CH_3), and 31 Da (–OCH_3), respectively.[43,51,52] Similarly, compound **21** showed the same fragmentation pattern as compound **18**, with fragment ions at *m/z* 295, 280, and 264.[43]

The molecular ion *m/z* 356 $[M + H]^+$ (Figure S17, SI section) was associated with compound **17**, annotated as tetrahydropalmatine, an alkaloid of the tetrahydroprotoberberine type, already described for the Annonaceae family.[59] According to Jiao *et al*.,[45] the fragment ion at *m/z* 192 was produced by RDA cleavage fragmentation at 8,13-position of the C-ring, and the fragment ion at *m/z* 192 generated the minor ion at *m/z* 177 by the loss of methyl group.

Alkaloid **20**, molecular ion *m/z* 296 $[M + H]^+$ (Figure S20, SI section), was suggested as xylopine, already reported for species of the genus.[46,56,60] Fragment ion at *m/z* 279 was produced after the loss of NH_3. Furthermore, additional fragment ions at *m/z* 249 and 221 were also generated. According to Macedo *et al*.,[51] the loss of 30 Da followed by 28 Da indicates the contraction of rings A or D.

Proanthocyanidins, also known as condensed tannins or procyanidins, constituted exclusively by catechin and/or epicatechin, were identified in the extract and acetate fraction of *A. tomentosa*. It was possible to observe typical procyanidin fragmentation patterns after quinone methide (QM), Retro-Diels-Alder (RDA), and heterocyclic ring fission (HRF).

Compounds **1**, **2,** and **12** were proposed as procyanidin dimers type B, with molecular ion *m/z* 577 $[M - H]^-$ (Figures S1, S2 and S12, SI section). It was possible to identify characteristic ions at *m/z* 451 ($[M - 126 - H]^-$), 425 ($[M - 152 - H]^-$) and 407 ($[M - 152 - 18 - H]^-$). It was possible to observe the fragment *m/z* 289, derived from the terminal unit after QM, which indicates the constitution of compounds by monomers ((epi)catechin).[40]

Compound **5**, *m/z* 865 $[M - H]^-$ (Figure S5, SI section), presented fragment ions at *m/z* 847 $[M - H - H_2O]^-$, 695 [M – H – gallic acid]$^-$ and 577 [M – H – 288]$^-$ after the loss of monomer.[42] It was suggested as a type B procyanidin trimer. Furthermore, the monomer (catechin) was also proposed in *A. tomentosa*. Catechin (compound **10**), *m/z* 289 $[M - H]^-$ (Figure S10, SI section), presented fragments characteristic of MS^2 and MS^3 at *m/z* 245 (neutral loss of CO_2), 205 and 203 (cleavage of the A-ring of flavan-3-ol), and 179, which may be associated with the loss of the B ring.[47-49]

In addition to the analysis of the raw data (MS^2 and MS^3 spectra), an undirected analysis was carried out using mass spectrometry data with the GNPS platform to assist in the chemical characterization and evaluate the variability of classes and subclasses of secondary metabolites, taking into account the few reports in the literature on the chemical profile of the species. In this way, the MS results were correlated with the molecular network (Figure 4). A manual inspection of the raw data was carried out in order to compare and confirm the annotations of the 20 annotated compounds (Table S1, SI section).

The MS/MS spectra were acquired in low-resolution mass spectrometers (LC-ESI-IT-MS), according to the fragmentations illustrated in Table S1 (SI section). The annotated compounds have a cosine value greater than or equal to 0.7, representing the MS/MS spectral similarity between sample spectra and spectra in the library. The

literature states that the closer to 1, the more similar the spectra are.[61]

Figure 4 presents the six molecular networks of spectral families generated after manually evaluating the annotated compounds through mass spectra. From the analysis of molecular clusters, it was possible to verify that alkaloids are the predominant classes of natural products of *A. tomentosa*, present mainly in the alkaloid fraction. This result corroborates the proposed structural elucidation. However, the annotation method is not considered an identification, only a tool to suggest the presence of compounds, and all results need to be compared with the literature. The non-targeted analysis does not assert the position of double bonds or substituents or support information about asymmetric centers. Thus, to identify and confirm a compound, it is necessary to use other spectrometric techniques.

After the chemical characterization in the present study and considering the different biological activities already described for species of the *Annonaceae* genus, we investigated the antitumoral potential of *A. tomentosa* against breast cancer cells *in vitro*. The current research explores the inhibitory properties of the methanol extract and the fractions of *A. tomentosa* against breast (MCF-7) cell proliferation and migration. To that end, we employed the 3D model of cell culture and correlated the results of the functional assays with the chemical compositions of the *A. tomentosa* extract and fractions.

Resazurin viability assay

The results obtained in the resazurin assay in 3D culture are shown in Figure 5a for the methanolic extract, Figure 5b for ethyl acetate fraction, and Figure 5c for the alkaloid fraction of the *Annona tomentosa*. After 72 h treatment (Figure 5a), the methanol extract (≥ 200 μg mL^{-1}) decreased cell viability when compared to SV. By analyzing the results of the ethyl acetate and alkaloid fraction at 72 h, the cell viability did not change in relation to SV after all treatment concentrations.

At the end of the resazurin assay (96 h), the fluorochromes HO and PI were added to assess the cell viability of the MCTS. The methanolic extract (10-100 μg mL^{-1}) did not change the viability by the resazurin assay and did not change the PI fluorescence intensity, which indicates cell death. However, the extract (50 and 100 μg mL^{-1}) decreased the intensity of HO fluorescence that marks cell nuclei (Figure 5d). At concentrations > 100 μg mL^{-1} of the methanolic extract, the spheroids did not retain the labeling with the fluorochromes, and it was impossible to analyze the fluorescence intensity. These data may indicate agreement with the results of resazurin, which demonstrated a decrease in cell viability at these concentrations. The fractions did not change the viability by the resazurin assay nor the PI fluorescence intensity. However, the alkaloid fraction (10-250 μg mL^{-1}) reduced the HO fluorescence (Figures 5e and 5f, respectively for ethyl acetate and alkaloid fractions).

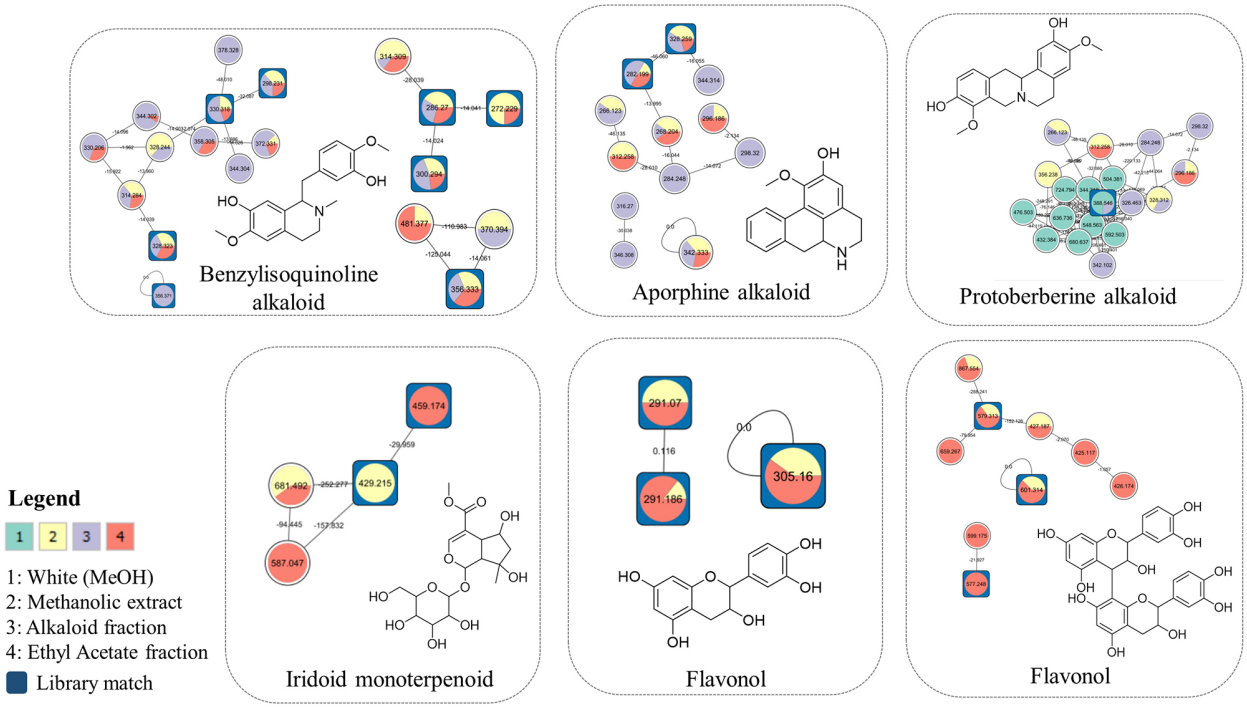

Figure 4. Molecular families obtained from classical molecular networking and annotated based on spectral matches within the GNPS platform. Each node represents a tandem mass spectrometry spectrum (MS/MS), while the edges that connect them represent the MS/MS fragmentation similarity (cosine > 0.7).

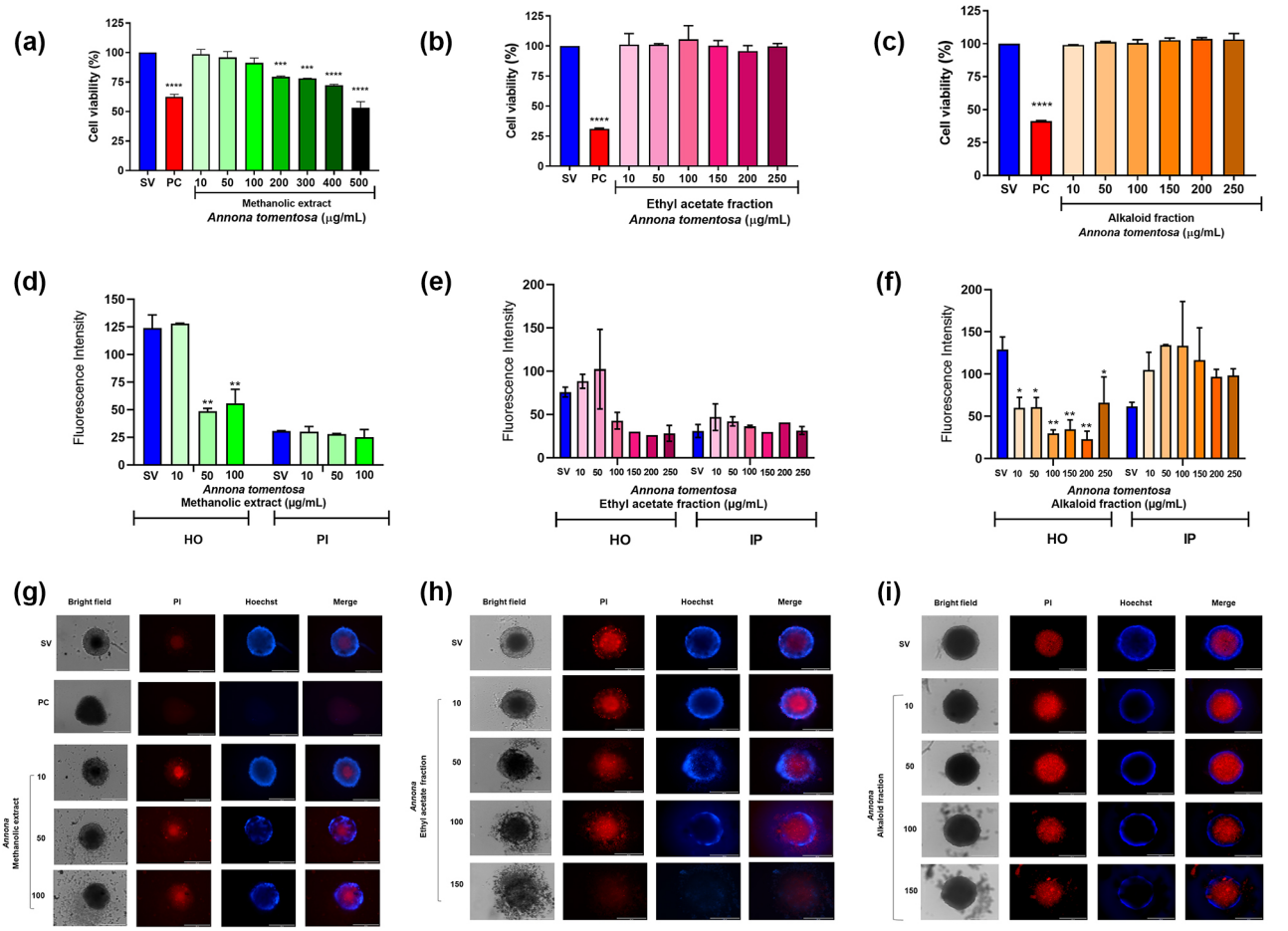

Figure 5. Cell viability (%) of MCF-7 MCTS evaluated using resazurin assay after treatment with (a) methanolic extract (10, 50, 100, 200, 300, 400, and 500 µg mL^{-1}), (b) ethyl acetate, and (c) alkaloid fractions (10, 50, 100, 150, 200, and 250 µg mL^{-1}) of *Annona tomentosa* after 72 h of treatment. Data are mean ± standard deviation. ANOVA and Dunnett's multiple comparisons tests. *$p < 0.05$, **$p < 0.01$, ***$p < 0.001$, ****$p < 0.0001$. SV: solvent vehicle (DMSO 0.25%); PC: positive control (docetaxel 100 µM). Representative images of MCF-7 spheroids treated with (g) methanolic extract, (h) ethyl acetate, and (i) alkaloid fractions of Annona tomentosa after 72 h treatment. PI: propidium iodide; scale bar = 400 µm.

Figures 5g, 5h, and 5i show representative fluorescence images of spheroids labeled with HO and PI and treated with methanolic extract, ethyl acetate, and alkaloid fractions, respectively.

In vitro approaches such as 3D models are robust and possess translational capabilities, in addition to being convenient, time-saving, and streamlined.[62] Our research group recently reviewed 3D cell culture models for breast cancer studies. The cellular models mostly used are MCF-7 and MDA-MB-231 cells that generate MCTS differently in morphology, even if they have the same tissue origin.[63] As we can see in Figure 5 (bright field image of SV), the spheroids of MCF-7 are compact, rounded, and well-defined with the three typical zones: proliferative, quiescent, and necrotic core. Treatments with the extract and its fractions aim to prevent viable cells, from the proliferative and quiescent zone, from multiplying and migrating from the spheroid, thus preventing tumor growth and the metastasis process. The resazurin assay is an inexpensive, simple, and non-invasive test that has been useful for characterizing growing cell populations within the 3D culture.[64] In the present study, the resazurin assay was not a good cell viability parameter compared to fluorochromes labeling. The spheroids treated with the highest extract concentrations that did not retain the dyes due to cell disintegration still showed some viability in the resazurin assay; in addition, fractions-treated spheroids showed a decrease in Hoechst labeling.

Area, integrity, and morphology of the MCTS

The results obtained after analyzing the area, morphology, and integrity from MCF-7 breast tumor 3D spheroids after the treatments with the extract and its fractions by 216 h can be seen in Figure 6. The methanolic extract (Figure 6a) (100 µg mL^{-1}) originated MCTS larger and less compact than the SV. In contrast, the 200 µg mL^{-1} treatment initially increased (144 h), followed by a

significant decrease (216 h) in the MCTS. At 300 μg mL^{-1}, no significant changes were observed in the 3D spheroids areas in the last treatment time, a similar growth pattern was observed in PC (DTX 100 μM). For the MCTS treated with the ethyl acetate fraction (Figure 6c), the spheroid area increased after 216 h treatment at concentrations of 50, 200, and 250 μg mL^{-1}. Finally, for MCF-7 tumor spheroids treated with the alkaloid fraction (Figure 6d) (> 150 μg mL^{-1}), a non-significant increase was observed up to 144 h, followed by disaggregation or a significant decrease in the MCTS.

At the end of the integrity test (216 h), resazurin was added to assess the cell viability of the MCTS. A significant drop in the cellular viability of the MCF-7 spheroids was observed in concentrations ≥ 50 μg mL^{-1} of the methanolic extract (Figure 6b) and 150 μg mL^{-1} to the alkaloid fraction (Figure 6e). When observing the percentages of cell viability, despite the extract having reduced cell viability as early as 72 h treatment, the alkaloid fraction reduced more effectively (ca. 50% for the extract and ca. 25% for the fraction) after 216 h. It was not possible to evaluate the MCTS viability for the ethyl acetate fraction.

We complemented the cell viability analysis using fluorescent markers. Viable cells are those in the proliferative and quiescent zone stained by Hoechst (DAPI/blue). The necrotic core/cells are marked by propidium iodide (red). The results showed in Figure 5g revealed that after 96 h of treatment, the methanolic extract treated MCTS (≥ 200 μg mL^{-1}), contrary to the results obtained with resazurin assay, were not viable anymore since they did not stain with fluorochromes, and the morphological changes were different when compared to the SV control. The images also show an increase in the necrotic core (red) compared to the SV. The ethyl acetate fraction did not reduce cell viability according to the resazurin

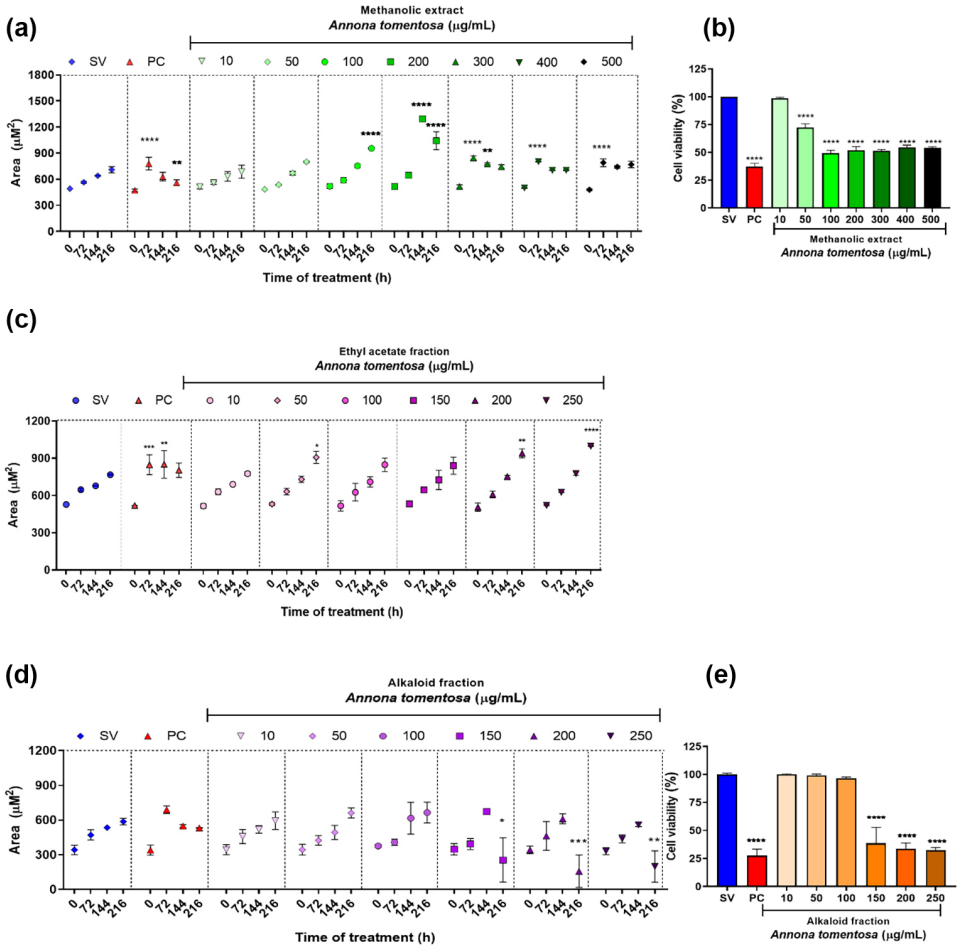

Figure 6. Volume (area μm^{-3}) occupied by MCF-7 3D tumor spheroids after 0, 72, 144, and 216 h of treatment with different concentrations of (a) methanolic extract (10, 50, 100, 200, 300, 400, and 500 μg mL^{-1}), (c) ethyl acetate, and (d) alkaloid fractions (10, 50, 100, 150, 200, and 250 μg mL^{-1}) of *Annona tomentosa*. Cell viability (%) of MCF-7 spheroids evaluated by resazurin assay after treatment with (b) methanolic extract and (e) alkaloid fraction of *Annona tomentosa* after 216 h of treatment. All values are presented as the mean ± standard deviation (X ± SD). Values statistically different from SV at the respective time point (day) (*$p < 0.05$; **$p < 0.01$; ***$p < 0.001$; ****$p < 0.0001$ ANOVA followed by Dunnett's post-test). SV: solvent vehicle (DMSO 0.25%), PC: positive control (docetaxel 100 μM).

assay; however, the images obtained after labeling with fluorochromes show that the fraction (≥ 50 μg mL^{-1}) decompressed the MCF-7 spheroids, which can be seen by the "dispersion" of the necrotic core. The alkaloid fraction was the one that most reduced the size of the 3D breast tumor spheroid, to the point of completely disintegrating it at concentrations ≥ 150 μg mL^{-1}.

3D clonogenicity assay

Figure 7 shows the results of the 3D clonogenicity assay obtained from disaggregated MCTS cells after 72 h of treatment with methanolic extract, ethyl acetate fraction, and alkaloid fraction. A significant reduction in the ability to form colonies was observed at all concentrations of the methanolic extract treatment (Figure 7a), except at the concentration of 10 μg mL^{-1}, where an increase in the SF was observed compared to the SV control. The ethyl acetate fraction (Figure 7b) reduced the clonogenic capacity after treatments with 10, 100, 150, 200, and 250 μg mL^{-1}. Interestingly, as we observed in the resazurin assay, the alkaloid fraction (Figure 7c) showed a more significant antiproliferative action when we observed the concentration of 100 μg mL^{-1} (ca. 48% for the extract and ca. 20% for the fraction) after 216 h.

The observed decrease in cellular viability following treatment with *A. tomentosa* extract and fractions indicates that they have cytotoxic effects on MCF-7 3D tumor spheroids and could have therapeutic potential against breast cancer. When we compared half-maximal inhibitory concentration (IC_{50}) values obtained after 72 h of treatment, the extract (IC_{50} = 824.2) decreased the cell viability more than fractions. For the fractions, it was impossible to calculate the IC_{50} because there was no reduction in viability at the evaluated concentrations. However, after 216 h of treatment, the alkaloid fraction had a lower IC_{50} (IC_{50} = 189.1) and completely disintegrated the MCTS. The clonogenic assay showed a more prominent effect of the alkaloid fraction.

Our results support studies that emphasize the anticancer effects of *Annona* species, attributed to the presence of bioactive compounds, including alkaloids and acetogenins.[2] *Annona squamosa* alkaloids, such as coclaurin, have demonstrated anti-tumoral activity against human breast (MCF-7) and colon (HCT116) cancer cells.[1] According to Nugraha *et al.*,[65] alkaloids from the *Annona* genus exhibit structural and pharmacological diversity, with the potential to promote anticancer and anti-infective therapies, such as anonaine, which has shown potent anticancer and cytotoxic activities against several human cancer cell lines *in vitro*. *In silico* analysis of anonaine alkaloid identified its potential to inhibit topoisomerase II, one of the main targets against cancer.[40]

The most relevant biological action of acetogenins is the inhibition of mitochondrial complex I due to its bis-tetrahydrofuran (bis-THF) structure. This inhibition relates to groups of pathways that can induce cell death through apoptosis and autophagy or act by inhibiting the enzyme lactate dehydrogenase A in other metabolic networks as an antioxidant or interrupting the cell cycle.[66] However, no compound of this class has been identified for *A. tomentosa*. In addition, flavonoids, terpenoids, and essential oils, among others, from species of the *Annona* genus presented antitumor and cytotoxic activities.[2] Hexane

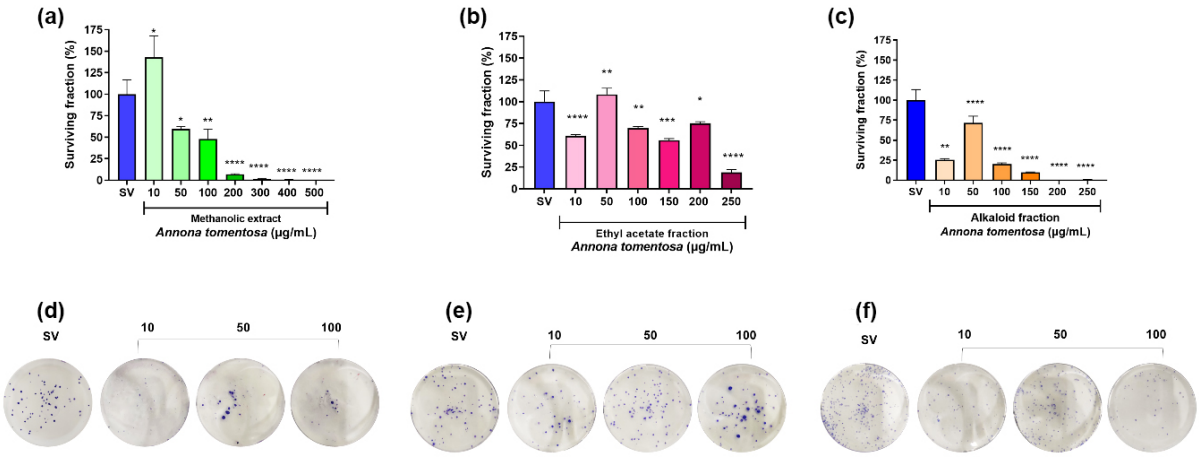

Figure 7. Clonogenic assay showing the surviving fraction (%) of MCF-7 cells disaggregated form 3D spheroids after treatment with (a) methanolic extract (10, 50, 100, 200, 300, 400, and 500 μg mL^{-1}), (b) ethyl acetate, and (c) alkaloid fractions (10, 50, 100, 150, 200, and 250 μg mL^{-1}) of *Annona tomentosa*. In the positive control group (docetaxel 100 μM), there was no formation of colonies (data not shown). All values are presented as the mean ± standard deviation (X ± SD). Values statistically different from SB at the respective time point (day) (*$p < 0.05$; **$p < 0.01$; ***$p < 0.001$; ****$p < 0.0001$ ANOVA followed by Dunnett's post-test). Solvent vehicle (DMSO 0.25%). (d), (e) and (f) representative images of the colonies in the different treatments. Positive control docetaxel 100 μM (not shown) did not form colonies.

partition from *Annona crassiflora* containing methylated catechin, acids palmitate, acetogenins and alkaloids in their constitution presented cytotoxicity and reduced the proliferative potential of cervical cancer cell lines.[67] The present study suggested catechin or epicatechin in *A. tomentosa*.

Cell migration in the extracellular matrix

The migration area was measured on images captured in a bright field (Figure 8). Treatments with the methanolic extract (50-500 μg mL^{-1}) and an alkaloid fraction (100-250 μg mL^{-1}) inhibited migration as observed for the positive control group (DTX), therefore being the samples with the highest anti-migratory/antimetastatic activity. The effects of the ethyl acetate fraction were less robust, with a significant anti-migratory effect only at concentrations of 150 and 200 μg mL^{-1}.

A representative image of each treatment with the alkaloid fraction (which exhibited the most significant anti-migratory effect) was also captured using Hoechst and PI staining to identify whether the migrated area was

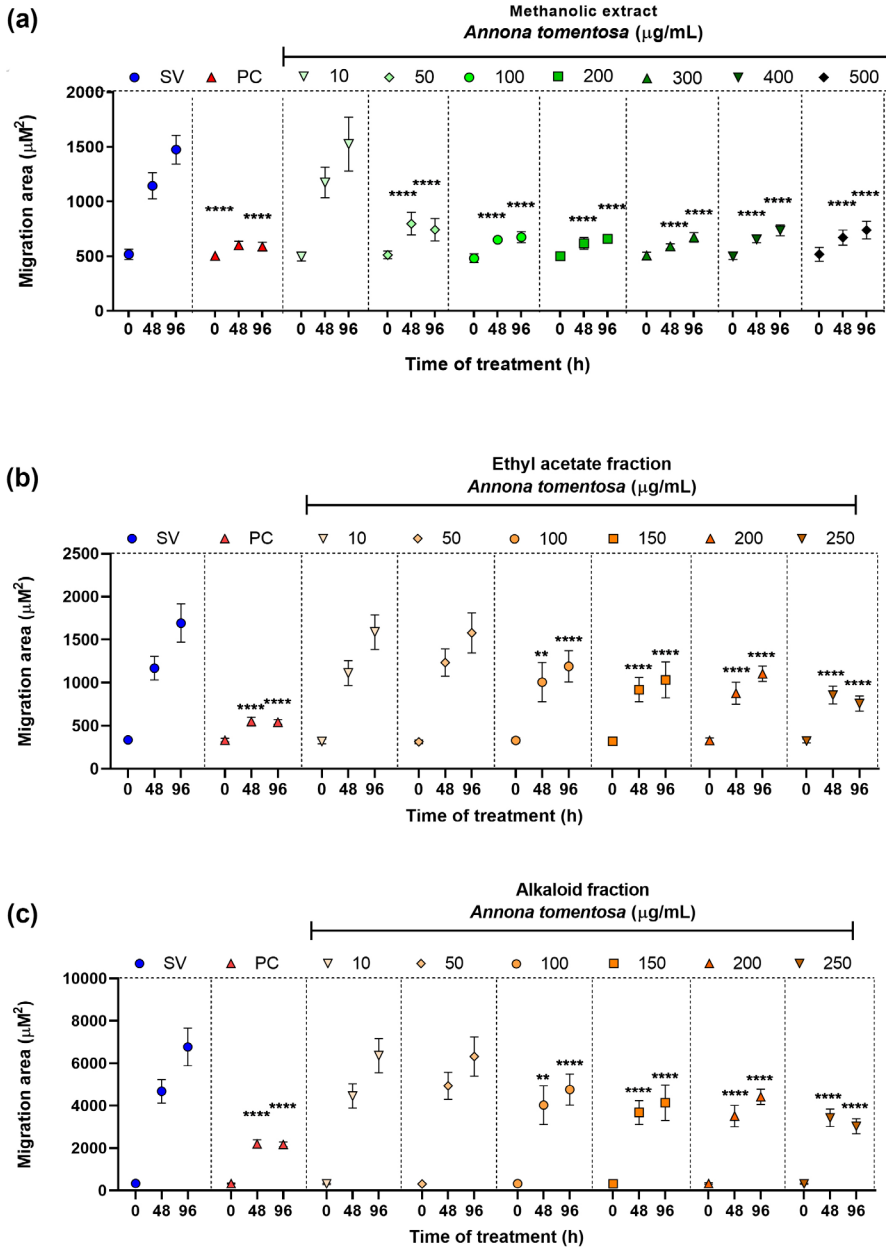

Figure 8. Cell migration area (μm^2) to the extracellular matrix (ECM) from MCF-7 3D spheroids 0, 48, and 96 h after treatments with (a) methanolic extract (10, 50, 100, 200, 300, 400, and 500 μg mL^{-1}), (b) ethyl acetate, and (c) alkaloid fractions (10, 50, 100, 150, 200, and 250 μg mL^{-1}) of *Annona tomentosa*. All values are presented as the mean ± standard deviation (X ± SD). Values statistically different from SV at the respective time point (day) (*$p < 0.05$; **$p < 0.01$; ***$p < 0.001$; ****$p < 0.0001$ ANOVA followed by Dunnett's post-test). SV: solvent vehicle (DMSO 0.25%).

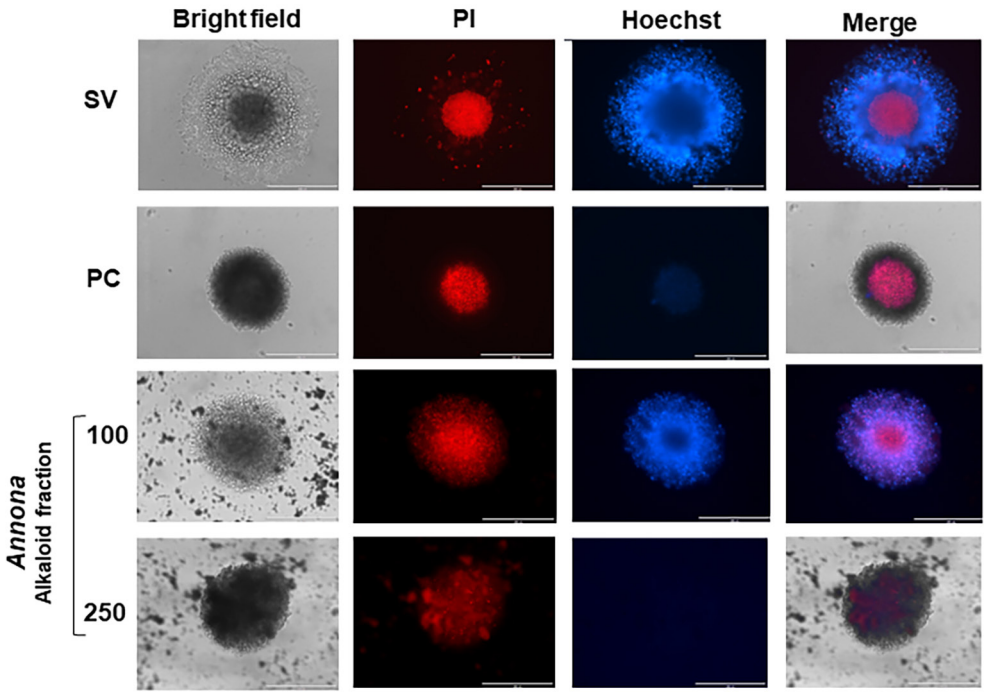

Figure 9. Representative images of MCF-7 tumor spheroids treated with alkaloid fraction of *Annona tomentosa* (10, 50, 100, 150, 200, and 250 μg mL^{-1}), solvent control (SV: DMSO 0.25%), and positive control (PC, docetaxel 100 μM) after 72 h of 3D cell migration in plates coated with extracellular matrix (gelatin). PI: propidium iodide; scale bar = 400 μm.

composed of living cells or cellular debris. As shown in Figure 9, despite a migration area in the highest concentration of the alkaloid fraction, the periphery cells were not marked by Hoechst, showing that it was just cell debris. At a concentration of 50 μg mL^{-1}, it is still possible to visualize viable cells in the periphery throughout the migration area, as observed in SV. However, in SV, cells in the periphery appear very little or no marked with PI, while the marking with PI is more significant at a concentration of 50 μg mL^{-1}.

In addition to the antiproliferative and cytotoxic effects presented in the present study and already reported in the literature for some species of *Annona* genus, the present study also demonstrated the potential of *A. tomentosa* to inhibit the migration of breast tumor cells from the MCTS. Antimigratory effects highlight a possible antimetastatic activity by preventing cells from migrating and reaching distant blood and lymphatic vessels and tissues. The *A. muricata* Linn leaf aqueous extract decreased the percentage of wound closure (43.9%) in the 4T1 breast cancer cell line besides inhibiting the cellular migration (100%) and invasion (44%) through the transwell membrane.[68] Antimigratory effects were also observed in wound healing assay in MCF-7 and MDA-MB-231 breast cancer cells treated with *A. squamosa* leaf extracts[12] and in HepG2 liver cancer cells treated with *A. crassiflora* fruit peel.[53] Sousa *et al.*[69] attributed the anti-migratory effects of acetogenins-rich fractions of *A. coriacea* to reduced cytoplasmic projections, decreased metalloproteinase 2 (MMP-2) activity in glioblastoma cell lines GAMG and U251MG.

Conclusions

This work is the first investigation of the chemical constituents with the help of the GNPS platform and of the biological activity regarding the cytotoxic and antiproliferative effects of *Annona tomentosa*. Our study is a pioneer in demonstrating the anticancer effects of the species and presenting results in the 3D culture model that best mimics the tumor microenvironment. The chemical profile mapping revealed that the species is a potential source of anticancer agents, especially alkaloids. To establish definitive insights into the biological impact on breast cancer MCF-7 cells and the structure-activity relationship of the compounds of this species, future endeavors should encompass further chemical studies dedicated to alkaloid isolation and characterization, along with pharmacological investigations.

Supplementary Information

Supplementary information (mass spectra, table and discussion of annotated compounds) is available free of charge at https://jbcs.sbq.org.br as a PDF file.

Acknowledgments

The authors thank the Coordination for the Improvement of Higher Education Personnel (CAPES; doctoral scholarship to Pereira, E.R., Finance Code 001 (Pinheiro, A. A.), PROCAD-AM (88887.472618/2019-00 (Rocha, C.Q.)) and FAPEMA ((Proc.: INFRA-02263/21 (Rocha, C.Q.)) and Brazilian National Council for Scientific and Technological Development (CNPq; Grant No. 404610/2021-8 to Serpeloni, J. M.; scientific initiation scholarship to Lee, C. Y. A. L. and Santos, A. G. P.) for supporting this study.

Author Contributions

AAP, CYALL, JMS, and CQR conceived the original idea, set the scope, and organized periodic discussions to develop and consolidate materials in this manuscript. CYALL; AGPS, and ERP carried out experiments, tabulated and described the results, and discussion regarding the biological activities of the extract and its fractions. AAP and MSR produced the extract and fractions and carried out the chemical composition analyses, tabulated and described their results and discussion. JMS, DLR and CQR coordinated, reviewed, and proofread the paper. All authors have critically reviewed and approved the final draft.

References

1. Al-ghazzawi, A. M.; *BMC Chem.* **2019**, *13*, 13. [Crossref]
2. Amala Dev, A. R.; Joseph, S. M.; *J. Indian Chem. Soc.* **2021**, *98*, 100231. [Crossref]
3. Zuo, C.; Zou, Y.; Gao, G.; Sun, L.; Yu, B.; Guo, Y.; Wang, X.; Han, M.; *Colloids Surf., B* **2022**, *213*, 112426. [Crossref]
4. Sung, H.; Ferlay, J.; Siegel, R. L.; Laversanne, M.; Soerjomataram, I.; Jemal, A.; Bray, F.; *Ca-Cancer J. Clin.* **2021**, *71*, 209. [Crossref]
5. Merino Bonilla, J. A.; Torres Tabanera, M.; Ros Mendoza, L. H.; *Radiologia* **2017**, *59*, 368. [Crossref]
6. Kashyap, D.; Pal, D.; Sharma, R.; Garg, V. K.; Goel, N.; Koundal, D.; Zaguia, A.; Koundal, S.; Belay, A.; *Biomed. Res. Int.* **2022**, *2022*, 1. [Crossref]
7. Moo, T.-A.; Sanford, R.; Dang, C.; Morrow, M.; *PET Clin.* **2018**, *13*, 339. [Crossref]
8. Waks, A. G.; Winer, E. P.; *JAMA* **2019**, *321*, 288. [Crossref]
9. Lovelace, D. L.; McDaniel, L. R.; Golden, D.; *J. Midwifery Womens Health* **2019**, *64*, 713. [Crossref]
10. Palesh, O.; Scheiber, C.; Kesler, S.; Mustian, K.; Koopman, C.; Schapira, L.; *Breast J.* **2018**, *24*, 167. [Crossref]
11. Salata, C.; deAlmeida, C. E.; Ferreira-Machado, S. C.; Barroso, R. C.; Nogueira, L. P.; Mantuano, A.; Pickler, A.; Mota, C. L.; de Andrade, C. B. V.; *Int. J. Radiat. Biol.* **2021**, *97*, 877. [Crossref]
12. Al-Nemari, R.; Bacha, A. Ben; Al-Senaidy, A.; Almutairi, M. H.; Arafah, M.; Al-Saran, H.; Abutaha, N.; Semlali, A.; *J. King Saud. Univ., Sci.* **2022**, *34*, 102013. [Crossref]
13. Swantara, M. D.; Rita, W. S.; Dira, M. A.; Agustina, K. K.; *Vet. World* **2022**, 124. [Crossref]
14. Vikas, B.; Anil, S.; Remani, P.; *Asian Pac. J. Cancer Prev.* **2019**, *20*, 2831. [Crossref]
15. Hadisaputri, Y. E.; Habibah, U.; Abdullah, F. F.; Halimah, E.; Mutakin, M.; Megantara, S.; Abdulah, R.; Diantini, A.; *Breast Cancer: Targets Ther.* **2021**, *13*, 447. [Crossref]
16. Younes, M.; Ammoury, C.; Haykal, T.; Nasr, L.; Sarkis, R.; Rizk, S.; *BMC Complementary Med. Ther.* **2020**, *20*, 343. [Crossref]
17. Oliveira, W.; Colares, L. F.; Porto, R. G.; Viana, B. F.; Tabarelli, M.; Lopes, A. V.; *Sci. Total Environ.* **2023**, *912*, 169147. [Crossref]
18. Carneiro, L. U.; da Silva, I. G.; de Souza, M. E. A.; Côrtes, W. S.; de Carvalho, M. G.; Marinho, B. G.; *J. Integr. Med.* **2017**, *15*, 379. [Crossref]
19. Santos, D. Y. A. C.; Salatino, M. L. F.; *Phytochemistry* **2000**, *55*, 567. [Crossref]
20. Matos, F. J. A.; *Introdução à Fitoquímica Experimental*, 3rd ed.; UFC: Fortaleza, Brazil, 2009.
21. *LC Solution*, version 2.3; Shimadzu Corporation, Kyoto, Japan, 2018.
22. *Data Analysis*, version 4.3; Bruker, Massachusetts, USA, 2014.
23. Global Natural Product Social Molecular Networking (GNPS), https://gnps.ucsd.edu/ProteoSAFe/status.jsp?task=b34b9047da9e4bd08a109df98c870874, accessed in January 2024.
24. Wang, Z.; Li, J.; Chambers, A.; Crane, J.; Wang, Y.; *J. Agric. Food Chem.* **2021**, *69*, 555. [Crossref]
25. Shannon, P.; Markiel, A.; Ozier, O.; Baliga, N. S.; Wang, J. T.; Ramage, D.; Amin, N.; Schwikowski, B.; Ideker, T.; *Genome Res.* **2003**, *13*, 2498. [Crossref]
26. Fujiike, A. Y.; Lee, C. Y. A. L.; Rodrigues, F. S. T.; Oliveira, L. C. B.; Barbosa-Dekker, A. M.; Dekker, R. F. H.; Cólus, I. M. S.; Serpeloni, J. M.; *J. Toxicol. Environ. Health, Part A* **2022**, *85*, 521. [Crossref]
27. *Qimaging Pro*, version 7.1; Teledyne, Canada, 2013.
28. *Zen*, version 2.3; Zeiss, Oberkochen, Germany, 2016.
29. Walzl, A.; Unger, C.; Kramer, N.; Unterleuthner, D.; Scherzer, M.; Hengstschläger, M.; Schwanzer-Pfeiffer, D.; Dolznig, H.; *SLAS Discovery* **2014**, *19*, 1047. [Crossref]
30. Schindelin, J.; Arganda-Carreras, I.; Frise, E., Kaynig, V.; Longair, M.; Pietzsch, T.; Cardona, A.; *Nat. Methods* **2012**, *9*, 676. [Crossref]
31. Friedrich, J.; Seidel, C.; Ebner, R.; Kunz-Schughart, L. A.; *Nat. Protoc.* **2009**, *4*, 309. [Crossref]
32. Vinci, M.; Gowan, S.; Boxall, F.; Patterson, L.; Zimmermann, M.; Court, W.; Lomas, C.; Mendiola, M.; Hardisson, D.; Eccles, S. A.; *BMC Biol.* **2012**, *10*, 29. [Crossref]

33. Mikhail, A. S.; Eetezadi, S.; Allen, C.; *PLoS One* **2013**, *8*, e62630. [Crossref]
34. Ribeiro, D. L.; Tuttis, K.; de Oliveira, L. C. B.; Serpeloni, J. M.; Gomes, I. N. F.; Lengert, A. H.; da Rocha, C. Q.; Reis, R. M.; Cólus, I. M. de S.; Antunes, L. M. G.; *Pharmaceutics* **2022**, *14*, 963. [Crossref]
35. Patties, I.; Kortmann, R. D.; Menzel, F.; Glasow, A.; *J. Exp. Clin. Cancer Res.* **2016**, *35*, 94. [Crossref]
36. Franken, N. A. P.; Rodermond, H. M.; Stap, J.; Haveman, J.; van Bree, C.; *Nat. Protoc.* **2006**, *1*, 2315. [Crossref]
37. Vinci, M.; Box, C.; Zimmermann, M.; Eccles, S. A. In *Target Identification and Validation in Drug Discovery: Methods and Protocols*, vol. 986, 1st ed.; Moll, J.; Colombo, R., eds.; Springer: New York, USA, 2013. [Crossref]
38. *AxioVision*, version 3.1; Zeiss, Oberkochen, Germany, 2013.
39. *GraphPad Prism*, version 7.0; La Jolla, USA, 2016.
40. Pereira, V. V.; da Fonseca, F. A.; Bento, C. S.; Oliveira, P. M.; Rocha, L. L.; Augusti, R.; Mendonça Filho, C. V.; Silva, R. R.; *Rev. Virtual Quim.* **2015**, *7*, 2539. [Crossref]
41. Singh, A.; Bajpai, V.; Kumar, S.; Singh Rawat, A. K.; Kumar, B.; *J. Pharm. Anal.* **2017**, *7*, 77. [Crossref]
42. Bamawa, C. M.; Ndjele, L. M.; Foma, F. M.; *J. Nat. Prod. Resour.* **2016**, *2*, 86. [Crossref]
43. de Lima, B. R.; da Silva, F. M. A.; Soares, E. R.; de Almeida, R. A.; da Silva-Filho, F. A.; Barison, A.; Costa, E. V.; Koolen, H. H. F.; de Souza, A. D. L.; Pinheiro, M. L. B.; *J. Braz. Chem. Soc.* **2020**, *31*, 79. [Crossref]
44. Lin, Z.; Yang, R.; Guan, Z.; Chen, A.; Li, W.; *Phytochem. Anal.* **2014**, *25*, 485. [Crossref]
45. Jiao, Q.-S.; Xu, L.-L.; Zhang, J.-Y.; Wang, Z.-J.; Jiang, Y.-Y.; Liu, B.; *Molecules* **2018**, *23*, 274. [Crossref]
46. Lima, J. M.; Leme, G. M.; Costa, E. V.; Cass, Q. B.; *J. Chromatogr. B* **2021**, *1164*, 122493. [Crossref]
47. Sun, J.; Liang, F.; Bin, Y.; Li, P.; Duan, C.; *Molecules* **2007**, *12*, 679. [Crossref]
48. Bravo, M. N.; Silva, S.; Coelho, A. V.; Boas, L. V.; Bronze, M. R.; *Anal. Chim. Acta* **2006**, *563*, 84. [Crossref]
49. Stöggl, W. M.; Huck, C. W.; Bonn, G. K.; *J. Sep. Sci.* **2004**, *27*, 524. [Crossref]
50. Yan, R.; Wang, W.; Guo, J.; Liu, H.; Zhang, J.; Yang, B.; *Molecules* **2013**, *18*, 7739. [Crossref]
51. Macedo, A. L.; Boaretto, A. G.; da Silva, A. N.; Maia, D. S.; de Siqueira, J. M.; Silva, D. B.; Carollo, C. A.; *J. Braz. Chem. Soc.* **2021**, *32*, 1840. [Crossref]
52. Justino, A. B.; Florentino, R. M.; França, A.; Filho, A. C. M. L.; Franco, R. R.; Saraiva, A. L.; Fonseca, M. C.; Leite, M. F.; Espindola, F. S.; *PLoS One* **2021**, *16*, e0250394. [Crossref]
53. Nishiyama, Y.; Moriyasu, M.; Ichimaru, M.; Iwasa, K.; Kato, A.; Mathenge, S. G.; Chalo Mutiso, P. B.; Juma, F. D.; *Phytochemistry* **2004**, *65*, 939. [Crossref]
54. Hagel, J. M.; Facchini, P. J.; *Plant Cell Physiol.* **2013**, *54*, 647. [Crossref]
55. Han, X.; Lamshöft, M.; Grobe, N.; Ren, X.; Fist, A. J.; Kutchan, T. M.; Spiteller, M.; Zenk, M. H.; *Phytochemistry* **2010**, *71*, 1305. [Crossref]
56. Cárdenas, C.; Torres-Vargas, J. A.; Cárdenas-Valdivia, A.; Jurado, N.; Quesada, A. R.; García-Caballero, M.; Martínez-Poveda, B.; Medina, M. Á.; *Biomed. Pharmacother.* **2021**, *144*, 112263. [Crossref]
57. Perrone, A.; Yousefi, S.; Salami, A.; Papini, A.; Martinelli, F.; *Sci. Hortic.* **2022**, *296*, 110896. [Crossref]
58. Pérez, E. G.; Cassels, B. K. In *The Alkaloids: Chemistry and Biology*, vol. 68; Cordell, G. A., ed.; Elsevier: Oxford, 2010, ch. 10. [Crossref]
59. Leboeuf, M.; Cavé, A.; Bhaumik, P. K.; Mukherjee, B.; Mukherjee, R.; *Phytochemistry* **1980**, *21*, 2783. [Crossref]
60. Rocha, G. N. S. A. O.; Dutra, L. M.; Pinheiro, W. H. P.; Silva, F. M. A.; Costa, E. V.; Almeida, J. R. G. S.; *Biochem. Syst. Ecol.* **2021**, *97*, 104297. [Crossref]
61. Moura, M. S.; Bellete, B. S.; Vieira, L. C. C.; Sampaio, O. M.; *Rev. Virtual Quim.* **2022**, *14*, 214. [Crossref]
62. Nair, L.; Mukherjee, S.; Kaur, K.; Murphy, C. M.; Ravichandiran, V.; Roy, S.; Singh, M.; *Biochim. Biophys. Acta, Gen. Subj.* **2023**, *1867*, 130361. [Crossref]
63. Okuyama, N. C. M.; Ribeiro, D. L.; da Rocha, C. Q.; Pereira, É. R.; Cólus, I. M. S.; Serpeloni, J. M.; *Toxicol. Appl. Pharmacol.* **2023**, *460*, 116376. [Crossref]
64. Uzarski, J. S.; DiVito, M. D.; Wertheim, J. A.; Miller, W. M.; *Biomaterials* **2017**, *129*, 163. [Crossref]
65. Nugraha, A. S.; Damayanti, Y. D.; Wangchuk, P.; Keller, P. A.; *Molecules* **2019**, *24*, 4419. [Crossref]
66. Jacobo-Herrera, N.; Pérez-Plasencia, C.; Castro-Torres, V. A.; Martínez-Vázquez, M.; González-Esquinca, A. R.; Zentella-Dehesa, A.; *Front. Pharmacol.* **2019**, *10*, 783. [Crossref]
67. Silva, V. A.; Alves, A. L. V.; Rosa, M. N.; Silva, L. R.; Melendez, M. E.; Cury, F. P.; Gomes, I. N. F.; Tansini, A.; Longato, G. B.; Martinho, O.; Oliveira, B. G.; Pinto, F. E.; Romão, W.; Ribeiro, R. I. M. A.; Reis, R. M.; *Invest. New Drugs* **2019**, *37*, 602. [Crossref]
68. Najmuddin, S. U. F. S.; Romli, M. F.; Hamid, M.; Alitheen, N. B.; Rahman, N. M. A. N. A.; *BMC Complement. Altern. Med.* **2016**, *16*, 311. [Crossref]
69. Sousa, L. R.; Oliveira, A. G. S.; Arantes, A.; Junqueira, J. G. M.; Alexandre, G. P.; Severino, V. G. P.; Reis, R. M.; Kim, B.; Ribeiro, R. I. M. A.; *Molecules* **2023**, *28*, 3809. [Crossref]

Submitted: November 15, 2023
Published online: March 20, 2024